Applied Catalysis B: Environmental 226 (2018) 575–584

Contents lists available at ScienceDirect

Applied Catalysis B: Environmental

journal homepage: www.elsevier.com/locate/apcatb

Complete oxidation of formaldehyde over TiO_2 supported subnanometer Rh catalyst at ambient temperature

Xiucheng Sun[a,b], Jian Lin[a,*], Hongling Guan[c], Lin Li[a], Li Sun[a,b], Yuehan Wang[a], Shu Miao[a], Yang Su[a], Xiaodong Wang[a,*]

[a] State Key Laboratory of Catalysis, Dalian Institute of Chemical Physics, Chinese Academy of Sciences, Dalian 116023, PR China
[b] University of Chinese Academy of Sciences, Beijing 100049, PR China
[c] Research Center of Heterogeneous Catalysis and Engineering Science, School of Chemical Engineering and Energy, Zhengzhou University, Zhengzhou, 450001, PR China

ARTICLE INFO

Keywords:
Formaldehyde
Rhodium
TiO_2
Formates
Oxidation

ABSTRACT

Catalytic oxidation of formaldehyde (HCHO) to CO_2 and H_2O under ambient condition is highly desired for purifying indoor air quality. In this work, it was found for the first time that TiO_2 supported subnanometer Rh catalyst exhibited a remarkable activity with complete removal of HCHO at room temperature. The humidity under ambient condition can significantly improve the activity, stability and specific rates but result in lower activation energy for the oxidation of HCHO on this catalyst. A combination of characterizations, such as H_2 temperature programmed reduction, adsorption microcalorimetry and in situ diffuse reflectance infrared Fourier transform spectroscopy, demonstrated the importance of Rh species for the dissociative adsorption of O_2 and the key role of water on the oxidation of HCHO. The O atoms facilitated the transformation of HCHO adsorbed on TiO_2 into intermediate of formates, while the presence of water led to the production of hydroxyl probably from the reaction with the adsorbed O species, which promoted the decomposition of formates to CO_2. This study can provide an important implication into the design and fabrication of more economic Rh-based catalysts for ambient HCHO oxidation.

1. Introduction

Indoor air quality is an important indicator of environmental health and suitable residence. Formaldehyde (HCHO), which commonly emits from the widely used building and decorative materials, is regarded as one of the dominant pollutants in airtight houses [1]. Long-time exposure to HCHO, even with a few ppm, may induce health problems such as headache, nasal tumors, eye irritation, respiratory tract or cancer [2,3]. It is necessary to reduce the indoor concentration of HCHO or eliminate it to satisfy the stringent environmental regulations and human health needs. Various strategies, including pressure-swing adsorption, photochemical degradation and catalytic oxidation, have been explored so far [4–10]. Among these strategies, the catalytic oxidation to harmless CO_2 and H_2O is generally recognized as a promising green technique for HCHO abatement due to high removal efficiency, energy-saving consideration and environmental-friendly reaction conditions [11–13].

Up to now, various formulations of catalysts have been developed for the oxidation of HCHO, including transitional metal oxides (MnO_2, Co_3O_4, CeO_2, etc.) [14–17] and supported noble metals (Au, Pt, Pd, etc.) [18–24]. The transitional metal oxides usually suffered from much higher temperature (> 150 °C) to completely eliminate HCHO. Comparatively, the supported noble metal catalysts have been extensively studied at relatively low or even room temperatures. Among these catalysts, Pt-based ones have been considered as one of the most outstanding catalysts for HCHO elimination. Zhang et al. [25] earlier prepared a highly effective Pt/TiO_2 catalyst that could completely oxidize HCHO into CO_2 and H_2O at room temperature with the presence of 100 ppm HCHO. An et al. [21] reported that complete conversion of HCHO could be achieved at room temperature over Pt/Fe_2O_3 catalyst prepared by a colloid deposition route due to well dispersion of Pt and suitable interaction between Pt and iron oxide support. He et al. [26] recently synthesized the alkali-metal promoted Pt/TiO_2 catalyst with the atomically dispersed $Pt\text{-}O(OH)_x$ species as the active sites for HCHO oxidation. They proposed that the alkali metal facilitated the stabilization of OH species and promoted the elimination of CH_2O. Correspondingly, the support that was abundant with hydroxyl species attracted much attention, such as Pt/AlOOH, Pt/Ferrihydrite, $PtNi(OH)_x/\gamma\text{-}Al_2O_3$ and so on [27–30]. The OH species-rich FeO_x as support for Au or Na-promoted Pd/TiO_2 catalyst also provided satisfactory

* Corresponding authors.
E-mail addresses: jianlin@dicp.ac.cn (J. Lin), xdwang@dicp.ac.cn (X. Wang).

https://doi.org/10.1016/j.apcatb.2018.01.011
Received 18 September 2017; Received in revised form 4 January 2018; Accepted 5 January 2018
Available online 06 January 2018
0926-3373/

performance for ambient HCHO elimination despite of slightly lower activity than Pt based ones [31,32]. However, the other Pt group metals (PGM) as alternatives have been rarely explored in the elimination of HCHO. Particularly, the Rh-based catalysts are never reported for HCHO oxidation at room temperature probably due to not only the relatively higher price but also the much inferior activity [13,33,34]. There is still large space to improve the performance of Rh-based catalyst to realize complete elimination of HCHO under ambient condition.

It is well accepted that the synergism between metal components and oxide is crucial to achieve high performance for a catalyst. The rational design of catalyst configuration may provide unexpected catalytic behaviors. One classical example is Au-based catalyst which has been long time considered as inert one until the work of Haruta et al. [35]. They found that the Au species with size in a scale of 2–5 nm can exhibit unexpected performance for CO oxidation. Previously, we tried to make PGM as active as Au by tuning the interaction between PGM and support by either downsizing metal particle from nano to cluster or single-atom [36,37], or engineering the metal-metal oxide interfaces [38,39]. The very recent work reported that changing the dispersion of Rh species to subnano size of lower than 1 nm can lead to much higher performance for CO oxidation at cryogenic temperature, which was suggested to result from the facile activation of O_2 as Rh-O-O-Ti and CO on Ti sites over the Rh-TiO_2 interface [40]. Similar to CO oxidation, the HCHO oxidation also suffered from the complication of O_2 activation [10,41]. Meanwhile, the HCHO molecule can be dissociatively adsorbed on the catalyst in a form of surface CO species, which has been suggested as an intermediate during the oxidation of HCHO [42,43]. Therefore, we applied this newly synthesized Rh/TiO_2 catalyst to the oxidation of HCHO. It was found here that the catalyst with Rh loading of 1.5 wt% exhibited an unprecedentedly high activity with complete conversion of HCHO at room temperature. Furthermore, this catalyst owned a perdurable stability with the existence of moisture under practical condition. A series of characterizations such as X-Ray Diffraction (XRD), High-angle annular dark-field scanning transmission electron microscopy (HAADF-STEM), adsorption microcalorimetry, in situ diffuse reflectance infrared Fourier transform spectroscopy (in situ DRIFTS) were then exploited to illuminate the reasons for the excellent activity and stability.

2. Experimental section

2.1. Synthesis of Rh/TiO_2 catalysts

All chemical reagents are analytically pure and used without further refinement in this experiment. A series of Rh/TiO_2 catalysts with different Rh loadings from 0.5 to 1.5 wt% were synthesized by deposition-precipitation method as reported previously [40]. In detail, 1 g of TiO_2-P25 (Degussa) was dispersed into 100 mL ultrapure water and stirred for 30 min at 80 °C in a water-bath. Next, the $RhCl_3$ solution with corresponding concentration was added dropwise into the TiO_2 suspension at a rate of 3 mL min^{-1} under rigorous stirring, during which the pH value was stabilized at around 8 with an aqueous solution of 0.2 M NaOH. After stirring for 3 h and aging for 1 h, the suspension was filtered and washed by 1 L hot ultrapure water to get rid of the chloride ions (tested by $AgNO_3$ solution). Then the filter cake was dried at 80 °C overnight and calcined at 400 °C for 4 h, yielding the catalysts denoted as n wt% Rh/TiO_2 with n as Rh loading amount which was determined by the ICP results.

2.2. Measurements of catalytic performance

The activity measurement for the catalytic oxidation of HCHO over Rh/TiO_2 catalysts was performed in a continuous-flow fixed bed reactor under atmospheric pressure. 100 mg catalyst was loaded in a U-type quartz tubular sandwiched by quartz wool layers. Before switching on the feed gas, which contained 140 ppm HCHO, 20 vol% O_2 and 50% RH (relative humidity) by He balanced under ambient condition at a total flow rate of 50 mL min^{-1} corresponding to a space velocity of 30,000 mL h^{-1} g_{cat}^{-1}, the catalysts of Rh/TiO_2 were pretreated by 20 vol% H_2/He in a flow of 20 mL min^{-1} at 200 °C for 30 min and cooled to room temperature in He for 30 min. Then the reactants were introduced into the reaction tube, among which gaseous HCHO was generated by passing helium through paraformaldehyde container in a thermostatic water bath and water vapor was generated by introducing another stream of helium through a water bubbler at room temperature. Therein, the HCHO concentration was tuned by the flow rate of helium and the temperature of water bath. RH was controlled by the flow rate of helium going through water. To investigate the moisture effect, RH was changed from 0 to 75% by modulating the ratio of helium passing through the paraformaldehyde and water bubbling. Sometimes, to simulate the practical indoor environment, the concentration of HCHO was maintained at a low level of 14 ppm but raising the flow rate to 100 mL min^{-1} corresponding to WHSV of 60,000 mL h^{-1} g_{cat}^{-1}. The inlet and outlet gas compositions were monitored by an on-line gas chromatograph (Agilent 7890B) equipped with hydrogen flame ionization detector (FID) and Ni catalyst convertor which was used for converting carbon oxides quantitatively into methane before the detector. No other carbonaceous compounds except CO_2 were detected in the effluents over all catalysts. Therefore, the HCHO conversion was expressed as $[CO_2]_{out}/[CO_2]_{total}$ (Eq. (1)), where $[CO_2]_{out}$ was the concentration of CO_2 produced at a certain temperature and $[CO_2]_{total}$ represented the concentration of CO_2 in the outlet gas when HCHO was totally oxidized into CO_2. The concentration of HCHO was calculated by the external standardization through the calibrated curve of CO_2 which was determined by altering the CO_2 concentration. In this experiment, the HCHO concentration was controlled at around 140 ppm.

HCHO conversion (X_{HCHO}) was calculated by the Eq. (1):

$$X_{HCHO} = \frac{[CO_2]_{out}}{[CO_2]_{total}} \times 100\% \quad (1)$$

For kinetic measurements, apparent activation energies for HCHO oxidation over Rh/TiO_2 catalysts were calculated according to the Arrhenius equation. The specific reaction rates at a series of temperatures were measured by keeping the conversion lower than 15%. The reaction rate of HCHO was calculated by the Eq. (2):

$$r_{HCHO} = \frac{X_{HCHO} \cdot f_{HCHO}}{m_{cat} \cdot n} \quad (2)$$

Where f_{HCHO} was HCHO molar gas flow rate, and m_{cat} was the mass of catalyst in the fixed bed and n is the loading amount of Rh.

2.3. Catalyst characterization

Metal loadings of Rh/TiO_2 samples were detected by inductively coupled plasma spectrometer (ICP) on an IRIS Intrepid II XSP instrument (Thermo Electron Corporation). Brunauer-Emmett-Teller (BET) surface areas of the catalysts were measured by nitrogen adsorption-desorption isotherms at −196 °C using a Micromeritics ASAP 2010 apparatus. X-ray diffraction (XRD) patterns were collected with the equipment of PW3040/60 X'pert PRO (PANalytical) diffractometer with voltage and current of 40 kV and 40 mA, respectively, using Cu Kα (λ = 0.15432 nm) as a radiation source. The intensity data were recorded in the 2θ range from 10° to 80°.

High-angle annular dark-field scanning transmission electron microscopy (HAADF-STEM) observations were operated on a JEOL JEM-ARM200F equipped with a CEOS probe corrector, with a guaranteed resolution of 0.08 nm. The catalyst sample reduced by H_2 or after the stability test was suspended into ethanol with an ultrasonic dispersion and a few of droplets were deposited on a copper grid and dried out with an infrared lamp.

H_2 temperature-programmed reduction (H_2-TPR) experiment was

performed on an Auto Chem II 2920 instrument. The catalyst was firstly purged with He for 2 h at 120 °C to remove physically adsorbed water and carbonates on the surface. Then, the temperature was increased from −50 to 900 °C at a ramping rate of 10 °C min^{-1} at the atmosphere of 10 vol% H_2/Ar and the H_2 consumption data was collected by TCD.

Microcalorimetric measurements of O_2 adsorption were performed using a BT 2.15 heat-flux calorimeter (Seteram, France). Prior to the adsorption, the sample was pre-reduced by H_2 in a special treatment cell at a certain temperature. The adsorption experiment was conducted at 40 °C and the detailed procedures for microcalorimetric adsorption have been described earlier [44].

In situ diffuse reflectance infrared Fourier transform spectroscopy (DRIFTS) were recorded using a BRUKER Equinox 70 spectrometer, equipped with a MCT detector and operated at a resolution of 4 cm^{-1} for 128 scans. Before each measurement, the sample was reduced in situ by 20 vol% H_2/He at 200 °C for 30 min and then purged with He for 1 h. After cooling to room temperature, the background spectrum was collected. The gas of HCHO/He or HCHO/O_2/He was introduced into the reaction cell successively, and then a flow of He was purged. For another experiment, O_2 or O_2 + H_2O were introduced in sequence after HCHO adsorption. All the DRIFT spectra were recorded by subtracting the background.

3. Results

3.1. Catalytic performance for HCHO oxidation

HCHO conversions over a series of different loading Rh/TiO_2 catalysts together with pure TiO_2 were detected as a function of reaction temperature ranging from 20 to 80 °C. As shown in Fig. 1, over TiO_2 the HCHO conversion can be negligible in the test temperature range. Upon loading 0.5 wt% Rh, HCHO conversion is dramatically increased to 37% at 20 °C and 61% at 30 °C, suggesting that the Rh species play a major role in the removal of HCHO. Along with the increase of Rh loading to 1 wt%, the catalyst displays an excellent activity with HCHO conversion of 100% at 30 °C. Remarkably, as the loading rises up to 1.5 wt%, this catalyst can realize complete HCHO conversion at only 20 °C with a high concentration of 140 ppm HCHO and a WHSV of 30,000 mL h^{-1} g_{cat}^{-1}. It is worth noting that for Rh-based catalyst, it is reported for the first time to catalyze the oxidation of HCHO totally to CO_2 and H_2O at room temperature.

The stability of the 1.5 wt% Rh/TiO_2 catalyst in the oxidation of HCHO was then measured and the results were shown in Fig. 2. To demonstrate the stability, we increased the space velocity to avoid a 100% conversion of HCHO. It can be seen that a constant of around

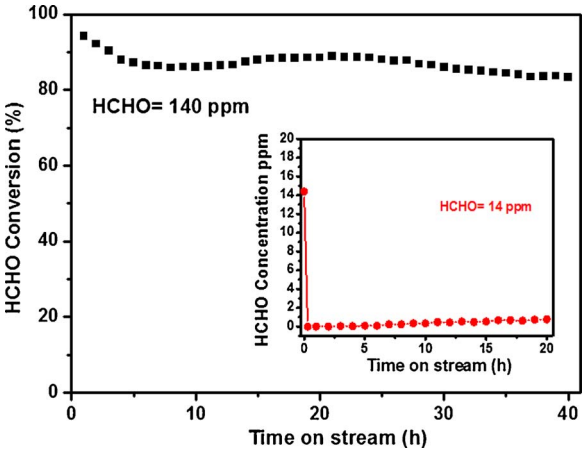

Fig. 2. Stability of HCHO oxidation over 1.5 wt% Rh/TiO_2 catalyst at 30 °C. Reaction conditions: 140 ppm HCHO, 20 vol% O_2, and balance He, RH: 50%, WHSV = 37,500 mL h^{-1} g_{cat}^{-1}. Inset figure: 14 ppm HCHO, 20 vol% O_2, and balance He, RH: 50%, WHSV = 60,000 mL h^{-1} g_{cat}^{-1}.

85% conversion with long term run of 40 h is found despite of the original slight decrease under the presence of 140 ppm HCHO at 30 °C. To mimic practical environmental condition, the concentration of HCHO in the feed gas is reduced to 14 ppm close to indoor situation and under a more stringent circumstance with an elevated WHSV of 60,000 mL h^{-1} g_{cat}^{-1}. This catalyst still exhibits satisfactory removal efficiency of HCHO to concentration of almost zero and good stability after 20 h run. Hence, the effective elimination and excellent stability in the removal of HCHO indicate high potential of Rh/TiO_2 catalyst in practical application.

Under ambient condition, the moisture is usually inevitable and the concentration changes with the climate. It is recognized that moisture has a positive or negative effect on the catalytic activity due to the formation of hydroxide species on the surface or the competitive adsorption with reactants. The influence of relative humidity of water on HCHO oxidation over 1.5 wt% Rh/TiO_2 catalyst was then studied. As shown in Fig. 3, when introducing dry HCHO feed gas without any humidity, the curve of HCHO conversion presents a reversed S-type descending from initially 72% to 15% after 20 h run. In detail, the HCHO conversion keeps a constant of ~70% in the first 4 h and rapidly decreases with time on stream until a platform of ~15% conversion. When adding water with RH of 25%, not only the removal efficiency is greatly enhanced to almost 90%, but also the catalyst exhibits much better stability over 20 h run. With further addition of RH to 50% and

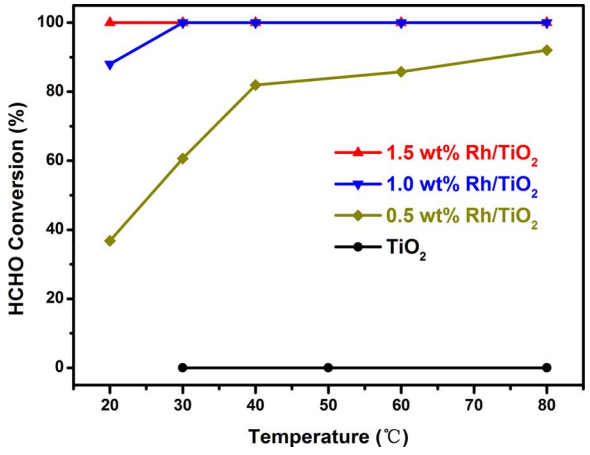

Fig. 1. HCHO conversions as a function of reaction temperatures on different Rh/TiO_2 and TiO_2 catalysts. Reaction condition: 140 ppm HCHO, 20 vol% O_2, and balance He, RH (relative humidity): 50%, WHSV (weight hourly space velocity): 30,000 mL h^{-1} g_{cat}^{-1}.

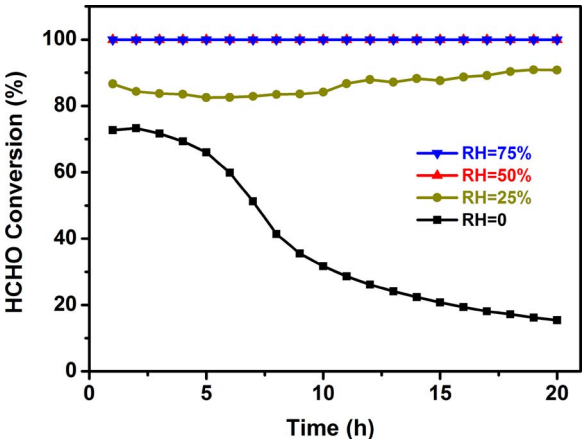

Fig. 3. Effect of relative humidity (RH) on HCHO conversion over 1.5 wt% Rh/TiO_2 catalyst at 40 °C. Reaction conditions: 140 ppm HCHO, 20 vol% O_2, He balance, WHSV = 30,000 mL h^{-1} g_{cat}^{-1}.

Table 1
Activity comparison of Rh/TiO_2 catalysts with the previously reported Rh based catalysts for HCHO oxidation in terms of specific rates and T_{50} values (temperature for 50% conversion of HCHO).

Catalyst	Rh loading (wt%)	Reaction condition	T (°C)	Specific rate (mmol g_{Rh}^{-1} h^{-1})	T_{50} (°C)	Note
Rh/TiO_2	1.5	140 ppm HCHO + 20% O_2 He balanced, RH = 50%	30	49.3	< 20	This work
Rh/TiO_2[a]	1.5	140 ppm HCHO + 20% O_2 He balanced, RH = 50%	30	24.0	–	This work
Rh/TiO_2-IMP[b]	1.5	140 ppm HCHO + 20% O_2 He balanced, RH = 50%	30	11.3	~30	This work
Rh/TiO_2	1.0	140 ppm HCHO + 20% O_2 He balanced, RH = 50%	30	46.1	< 20	This work
Rh/TiO_2	0.5	140 ppm HCHO + 20% O_2 He balanced, RH = 50%	30	22.8	< 30	This work
Rh/TiO_2	1.0	100 ppm HCHO + 20% O_2 He balanced	–	–	~55	Ref. [30]
Rh/TiO_2	0.6	100 ppm HCHO + 22% O_2 N_2 balanced	40	20.8	90	Ref. [29]
Rh/CeO_2	5.0	900 ppm HCHO + 160 ppm CH_3OH in air, RH: 18%	–	–	< 150	Ref. [41]

[a] The catalyst was calcined at 650 °C for 4 h. It was found previously that after this treatment the Rh size was increased to around 2 nm without the change of support composition [40].
[b] The Rh/TiO_2-IMP sample was prepared by incipient wetness impregnation method.

75%, the HCHO conversion keeps on a high level of 100% and no deactivation is detected during the long term run. The above result indicates that for Rh/TiO_2 catalyst, the existence of H_2O dramatically improves the elimination of HCHO probably due to the provision of hydroxyl groups. Moreover, the catalyst has good tolerance to high concentration of moisture, further convincing its practical capacity.

To show the intrinsic activity of these Rh/TiO_2 catalysts, the specific rates and T_{50} values for HCHO oxidation were examined and compared with the former Rh based catalysts. The results were displayed in Table 1. It is found that the specific rate of 1.5 wt% Rh/TiO_2 is as high as 49.3 mmol g_{Rh} h^{-1}. With the lower loading, this specific rate decreases correspondingly, indicating the importance of Rh species for the conversion of HCHO. When compared with other Rh based catalysts, this activity is times higher but working at lower temperature. With comparison of T_{50} values, we can see that it is ~55, 90, and < 150 °C over the former 1 wt% Rh/TiO_2 [34], 0.6 wt% Rh/TiO_2 [33], 5 wt% Rh/CeO_2 catalysts [45], respectively, while the corresponding value of our catalyst is below 20 or 30 °C. Therefore, our Rh/TiO_2 catalysts unequivocally possess much higher performance for the elimination of HCHO either in HCHO conversion or in specific rate. On the other hand, the apparent activation energy (Ea) of the Rh/TiO_2 catalyst for the oxidation of HCHO was also detected. As shown in Fig. 4, without the presence of humidity, i.e. RH = 0, the value of Ea is around 29 kJ mol^{-1}, while under the condition of RH = 50%, the reaction rate is improved with the lower Ea value of 23 kJ mol^{-1}. Coupled with the performance detect in Fig. 3, these results further demonstrate that the presence of humidity not only promotes the oxidation of HCHO but also results in a lower activation energy which implies that the reaction pathway or the rate-determining step changes in the presence of H_2O.

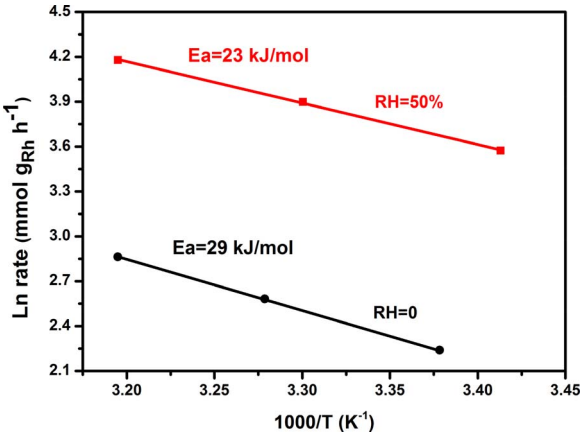

Fig. 4. Arrhenius plots for HCHO conversion over 1.5 wt% Rh/TiO_2 catalyst under conditions of RH = 0 and RH = 50%, respectively.

3.2. Structure characterization

The structure information of 1.5 wt% Rh/TiO_2 catalyst before and after test was detected. The BET surface areas and support crystal phase of the samples were listed in Table 2. All the catalysts exhibit similar BET surface areas and support properties with the original P25 support. In detail, Fig. 5 shows the XRD patterns of the support TiO_2 and the reduced or used catalysts. Typical peaks are observed at 2θ = 25.3° and 27.5° which belong to anatase (101) (JCPDS No.04-0477) and rutile (110) (JCPDS No.04-0551) crystal planar, respectively, indicating that all the supports are well-mixed P25 phases and there are no structural changes between catalysts of H_2 reduced and long-term reaction. Meanwhile, the characteristic peaks of Rh-containing phases for both the reduced and the used catalysts are not detected mainly due to the high dispersion of Rh species.

HAADF-STEM characterizations were examined to observe the dispersion of Rh species and the structure of support for the reduced 1.5 wt % Rh/TiO_2 catalyst and the one that was submitted to long-term run of HCHO oxidation. As shown in Fig. 6, obvious lattice fringes with the spacing of 0.184 nm and 0.323 nm are observed, corresponding to (200) plane of anatase TiO_2 and (110) plane of rutile one, respectively, which is consistent with the XRD results. Through analyzing the images with various magnifications in Fig. 6a–c, we find that the Rh species are uniformly dispersed on the two phases of anatase and rutile in subnano clusters with centralized size of 0.62 nm. For the catalyst after stability reaction as shown in Fig. 6d–f, the average size of Rh species is similar of ~0.7 nm. The high dispersion and stability of Rh species are favorable for the long-term run during the HCHO oxidation process.

Table 2
Physiochemical properties of TiO_2, the reduced and the used 1.5 wt% Rh/TiO_2 catalysts.

Sample	BET (m^2/g)	Composition[a] (%)		Crystal size[a] (nm)	
		Anatase	Rutile	Anatase	Rutile
TiO_2	60	83	17	22	33
1.5 wt% Rh/TiO_2-red	58	83	17	22	32
1.5 wt% Rh/TiO_2-used	62	82	18	23	33

[a] obtained from XRD detections.

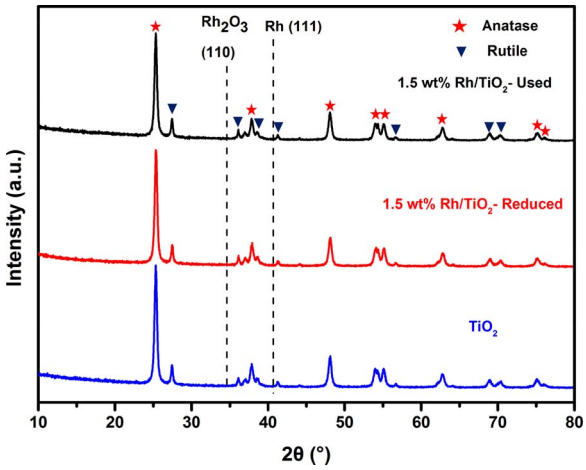

Fig. 5. XRD patterns of TiO_2, the reduced and the used 1.5 wt% Rh/TiO_2 catalysts.

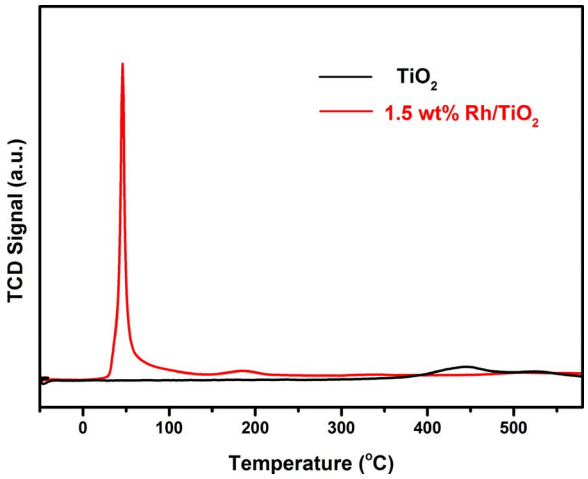

Fig. 7. H_2-TPR profiles of TiO_2 and 1.5 wt% Rh/TiO_2.

3.3. H_2-TPR and O_2 adsorption microcalorimetry

H_2-TPR experiments were carried out to investigate the reducibility of 1.5 wt% Rh/TiO_2 and pure TiO_2. As shown in Fig. 7 and Table 3, over TiO_2 there is only a broad and weak peak centered at a high temperature of 442 °C. In contrast, with the loading of Rh a sharp peak appears which arises from the temperature of 25 °C and centralized at 46 °C. The corresponding consumption amount of H_2 is 273 μmol g_{cat}^{-1} which is a little higher than the theoretical value for the reduction of Rh^{3+} to Rh^0 (218 μmol g_{cat}^{-1}), suggesting that all of Rh species together with the neighbouring TiO_2 have been reduced. There is a strong interaction between Rh species and TiO_2, which favors the high dispersion of Rh clusters and the production of surface oxygen vacancies on TiO_2.

The O_2 adsorption on the reduced 1.5 wt% Rh/TiO_2 and TiO_2 support is detected by a special microcalorimetric method which can quantitatively give adsorption heat and amounts [46]. As shown in Fig. 8, there is almost no adsorption of O_2 on the pure TiO_2 support. Comparatively, a plateau value of adsorption heat of around 340 kJ mol^{-1} with saturated adsorption amount of around 150 μmol g_{cat}^{-1} can be observed on this catalyst, similar to the heat of formation of Rh_2O_3 from oxidative to metallic Rh (343 kJ mol^{-1}) [47], suggesting that the main sites for O_2 adsorption are located on Rh species. The H_2-TPR detection shows a good reducibility of Rh species of Rh/TiO_2 from room temperature, which can be reoxidized by O_2 as obtained from the microcalorimetric study. All of these results suggest

Table 3
Reducibility of Rh/TiO_2 catalysts obtained by H_2-TPR.

Sample	Loadings (wt%)	H_2 consumption (umol g_{cat}^{-1})	
		Peak I (T_α/°C)[a]	Theoretical[b]
Rh/TiO_2	1.5	273 (46)	218
TiO_2	–	81 (442)	–

[a] The central reduction temperatures and H_2 consumption amounts.
[b] The theoretical H_2 consumption amount for Rh_2O_3 to Rh.

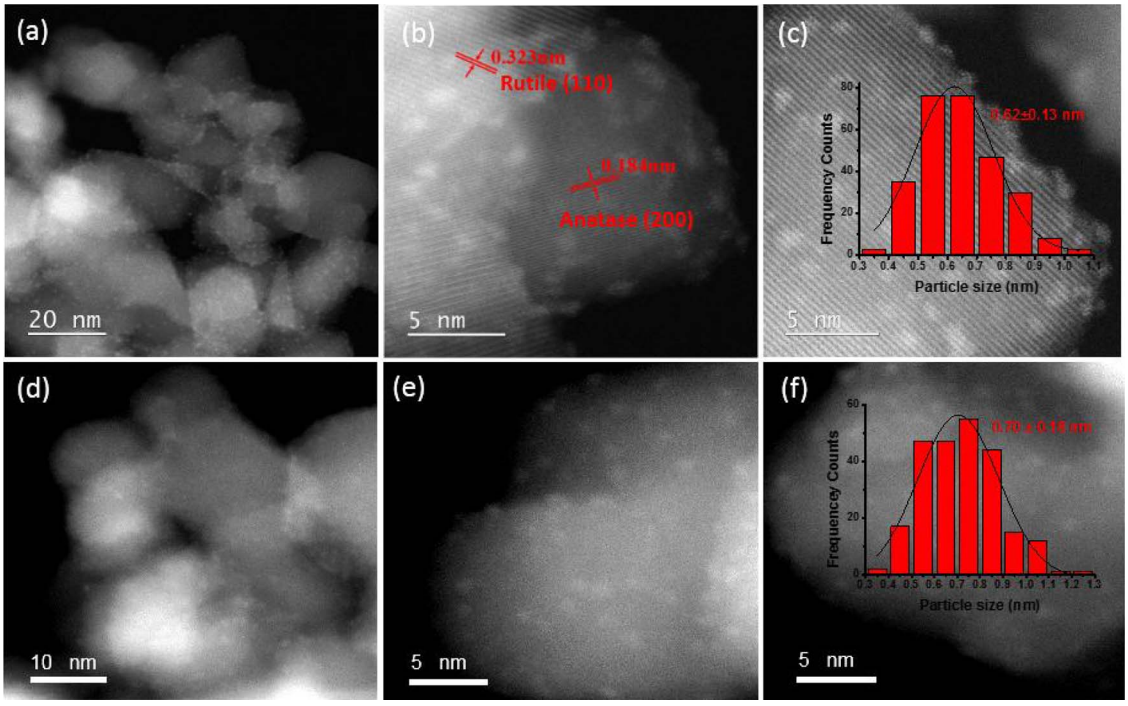

Fig. 6. Typical HAADF-STEM images of the reduced 1.5 wt% Rh/TiO_2 catalysts (a–c) and the used sample after the stability test (d–f).

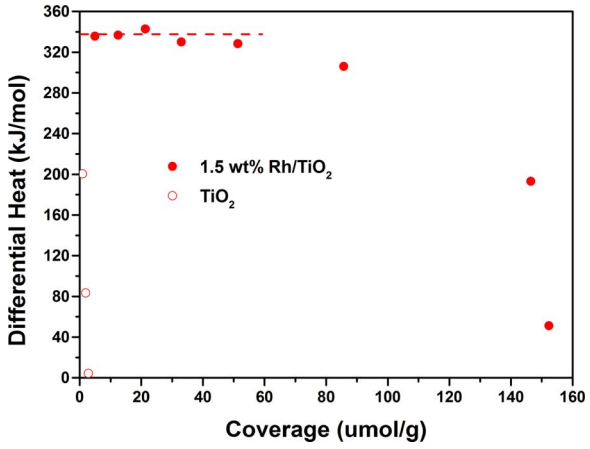

Fig. 8. Microcalorimetric results of O_2 adsorption on 1.5 wt% Rh/TiO_2 and TiO_2.

that the O_2 molecule can be dissociatively adsorbed on Rh sites to form O atoms.

3.4. In situ DRIFTS detections during HCHO oxidation

The in situ DRIFTS experiments were conducted to reflect the adsorption of HCHO and its reaction with O_2 or $O_2 + H_2O$. The spectra of HCHO adsorption on 1.5 wt% Rh/TiO_2 were obtained with the exposing time at room temperature. As shown in Fig. 9, with the introduction of HCHO, no peak at 1722 cm^{-1} can be found which is ascribed to the molecularly adsorbed HCHO [48]. While many other complex peaks appear, which can be distributed as listed in Table 4 as follows: peaks at 2069 and 1931 cm^{-1} are attributed to CO that comes from the dissociation of HCHO; peaks at 2954, 2925, 2869, 2846, 2825, 2738 cm^{-1} and also the strong peaks at 1571 and 1357 cm^{-1} are attributed to the stretching mode υ(CH) or δ(CH), υ_{as}(COO-) and υ_s(COO-) of formates, respectively; peaks at 1469 and 1128 cm^{-1} belong to the δ(CH_2) and υ(CO) of the dioxymethylene (DOM) species; and the peaks at 1310 and 1380 cm^{-1} belong to carbonate species [26,48–51]. Moreover, it should be noted that there is gradual decrease of peaks at 3675, 3453 and 1654 cm^{-1} with the time, which are assigned to hydroxyl species. These results suggest the quick transformation of HCHO after its adsorption on this catalyst coupled with the participation of OH species during this transformation process. On the other hand, we find that the adsorption of HCHO on the pure TiO_2 also results in the presence of peaks attributed to formates, DOM and carbonates, similar with those on Rh/TiO_2 except that of CO peaks in Fig. 10a. It is clear that the support of TiO_2 supplies the sites for the transformation of HCHO into the dominant intermediate of formates or DOM via interaction with the OH groups while the Rh sites for the adsorbed CO species.

The sample with saturated adsorption of HCHO was then consecutively exposed to the flow of helium, O_2 and finally $O_2 + H_2O$ to demonstrate the reactivity of these intermediates. As shown in Fig. 11, the CO peaks do not change any after the purging by helium, indicating no decomposition of formates or DOM to form CO on our Rh/TiO_2, the phenomenon of which was found during HCHO oxidation on Pt/TiO_2 catalyst and considered as a rate-determining step [42]. With the introduction of O_2, no change of CO peaks happens. Instead, the vibration bands of DOM at 1469 and 1128 cm^{-1} almost disappear which might be converted into the formates [29]. Moreover, there is slight increase of peak strength at 3675 cm^{-1} and appearance of peak at 1654 cm^{-1} as shown in the inset figure of Fig. 11, which indicates the production of OH groups from the oxidation of small quantity of DOM [50]. Comparatively, O_2 does not induce any change of peaks on TiO_2 when it is introduced to the HCHO preadsorbed TiO_2 sample as shown in Fig. 10b. These results suggest that it is the dissociated adsorbed O atoms on Rh sites that promote the formation of formates by dehydrogenation reaction of HCHO. These O atoms can also favor the conversion of formates to CO_2 but only in a limited extent. With the further introduction of $O_2 + H_2O$ on Rh/TiO_2, the peaks at 3675, 3453 and 1654 cm^{-1} significantly increase, indicating the production of OH species. Correspondingly, the peaks at 2954, 2925, 2869, 2846, 2738 cm^{-1} immediately disappear coupled with remarkable decrease of peak strength at 1571 and 1357 cm^{-1}, indicating the facile decomposition of these species under the presence of $O_2 + H_2O$. In contrast, there is no shift or strength weakening of CO peaks. In this regard, the formates play as an important intermediate and water promotes the conversion of formates due to the effect of OH species from reaction between adsorbed O and H_2O [38,52], which is more favorable than the adsorbed O atoms for the oxidation of HCHO to CO_2.

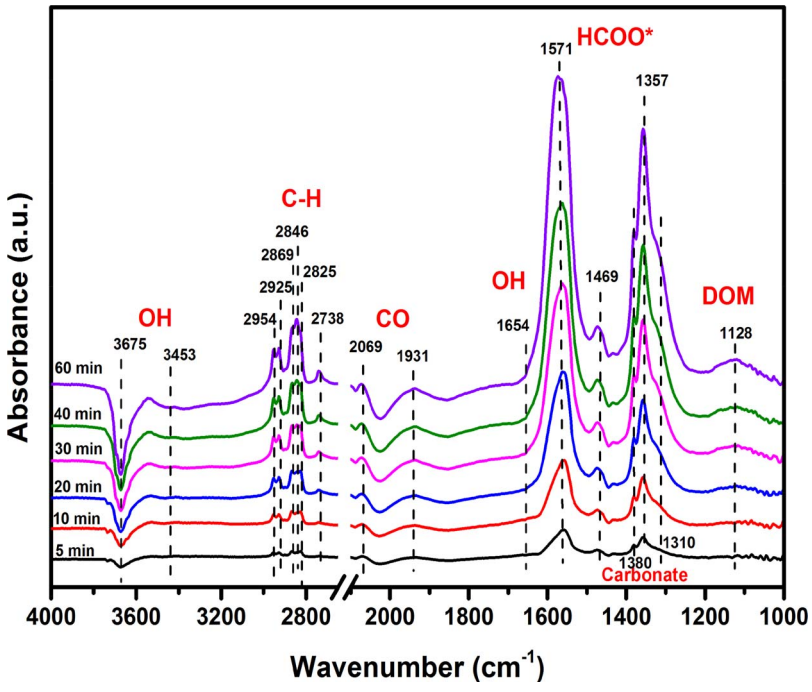

Fig. 9. In situ DRIFT spectra after introducing HCHO to 1.5 wt% Rh/TiO_2 with time on stream at room temperature.

Table 4
IR bands after the adsorption of HCHO on the Rh/TiO_2 catalyst.

IR band wavenumber (cm^{-1})										
−OH		C−H			CO	HCOO−		DOM		Carbonates
ν(OH)	δ(OH)	ν_{as}(CH)	ν_s(CH)	δ(CH)	ν(CO)	ν_{as}(OCO)	ν_s(OCO)	δ(CH_2)	ν(CO)	$\nu(CO_3)$
~3675 ~3453	~1654	~2846 ~2825	~2925 ~2869	~2954 ~2738	~2069 ~1931	~1571	~1357	~1469	~1128	~1380 ~1310

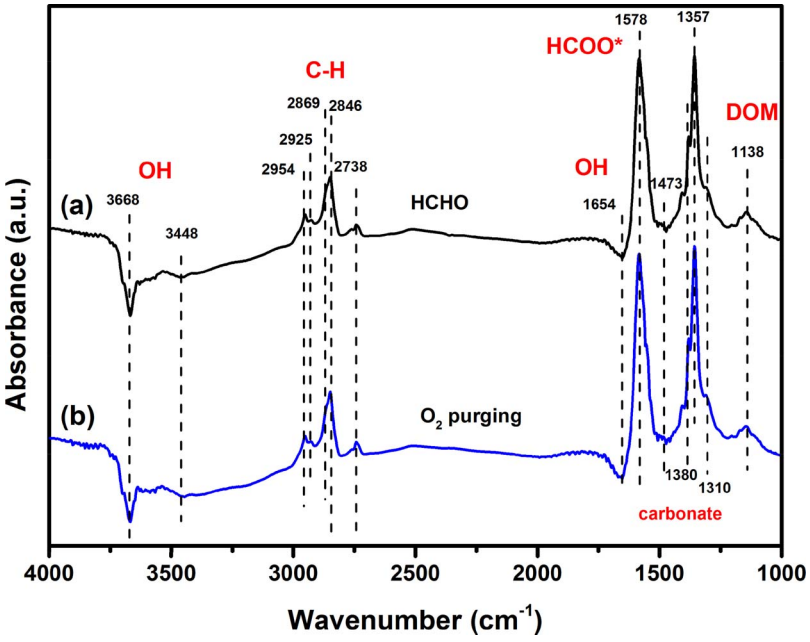

Fig. 10. In situ DRIFT spectra under steady condition with HCHO adsorption (a) and then submitted to O_2 (b) on TiO_2 at room temperature.

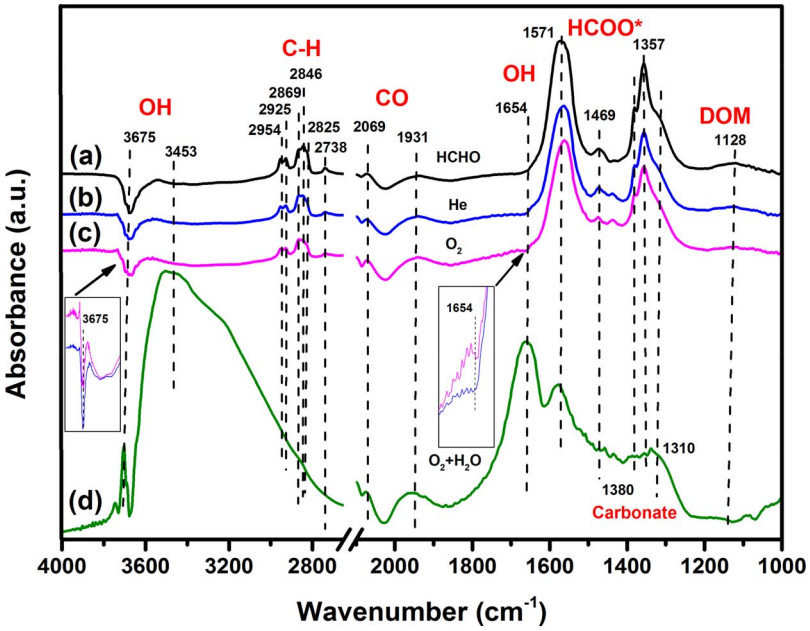

Fig. 11. In situ DRIFT spectra of introducing HCHO (a), then He (b), O_2 (c), and finally O_2 + H_2O (d) over 1.5 wt% Rh/TiO_2 catalyst. Inset figure: the amplified region of the peaks at 3675 and 1654 cm^{-1}.

4. Discussion

There is a common recognition that Rh based catalysts exhibited much inferior performance among the noble metals for ambient oxidation of HCHO so far [12,13]. However, it is interesting to find here that the Rh/TiO_2 catalyst exhibits complete oxidation of HCHO at room temperature with a good stability and lower activation energy, which is even comparable with the extensively studied Pt based catalyst for room-temperature oxidation of HCHO. It should be noted that this catalyst was synthesized by a deposition-precipitation method by which the possible negative effect of the Cl^- species on the activity of HCHO oxidation could be avoided, while the traditional Rh based catalysts

were mostly prepared by an impregnation method in which most of the Cl^- in the precursor remained in the catalyst [33,34]. It was found that the Cl^- could poison the metal nanoparticles by the coordination bonds with surface metal atoms, leading to the prohibition of oxygen adsorption and activation [53]. For comparison, we also prepared the 1.5 wt% Rh/TiO_2 catalyst with incipient wetness impregnation method (Rh/TiO_2-IMP) for the oxidation of HCHO under the same reaction condition. As shown in Table 1, the T_{50} value is higher of ~30 °C and the specific reaction rate is lower of 11.3 mmol g_{Rh}^{-1} h^{-1} on 1.5 wt% Rh/TiO_2-IMP compared with those on the Rh/TiO_2 catalyst prepared by the deposition-precipitation method. In addition, the metal particle size was identified as a vital factor for the catalytic performance [54,55]. When the Rh size on 1.5 wt% Rh/TiO_2-650 is increased to around 2 nm, the reaction rate for HCHO oxidation is lowered to 24.0 mmol g_{Rh} h^{-1}, around half amount of the value (49.3 mmol g_{Rh} h^{-1}) on Rh species with size of 0.62 nm as listed in Table 1. Moreover, the specific rate is also around half value (22.8 mmol g_{Rh} h^{-1}) on 0.5 wt% Rh/TiO_2 with dispersion of mainly single-atoms or pseudo single-atoms [40]. These results illustrate that the Rh subnano clusters are critical for the high efficiency of HCHO removal. Thus the subnanometer Rh species dispersed on TiO_2 without the presence of Cl^- make it highly active in the oxidation of HCHO at room temperature.

The role of TiO_2 and subnanometer Rh species and the mechanism of HCHO oxidation on Rh/TiO_2 are then discussed. TiO_2 can supply the sites for HCHO adsorption and the presence of OH species facilitates the transformation of the adsorbed HCHO as shown in Figs. 9 and 10. The Rh species favor the dissociative adsorption of O_2 into O atoms according to microcalorimetric result of Fig. 8. These O atoms can even promote the transformation of HCHO into intermediate formates by comparison of DRIFT spectroscopy in Fig. 12a under the conditions of introducing HCHO + O_2 and HCHO on 1.5 wt% Rh/TiO_2, respectively. Through the quantitative analysis in Fig. 12b, it is found that the formation rate of formates is around 4 times higher during the adsorption of HCHO + O_2 than that of HCHO by integrating the typical peak at 1571 cm^{-1}, which can be considered as a representative of formates [30,56]. Coupled with the results of Fig. 11, the faster generation of formates can result from the promotion of dehydrogenation of HCHO or DOM by surface O atoms [29,57]. Furthermore, the presence of H_2O greatly facilitates the HCHO oxidation at room temperature and improves the stability over Rh/TiO_2. It has been suggested that the dissociated O atoms on the metal surface could readily react with the adsorbed water molecule to form OH groups, i.e. $O_{ad} + H_2O_{ad} \rightarrow 2OH$ [58]. Particularly, the oxygen vacancies on the reduced TiO_2 neighbored with Rh species favored the process of OH formation [59]. The results in Fig. 11 point out that the OH species are more favorable for the decomposition of formates to CO_2 than the O species and do not change the CO peaks on Rh sites. These results indicate that the high performance of Rh/TiO_2 for the oxidation of HCHO results from the reaction between intermediate of formates and OH species rather than that between intermediate of CO and O species, although this catalyst exhibited unexpected activity for CO oxidation as studied in our previous work [40].

The possible reaction mechanism for the HCHO oxidation under humidity condition over Rh/TiO_2 is then proposed as depicted in Fig. 13. Firstly, the HCHO molecule is adsorbed on TiO_2 via the hydrogen bonding of the surface OH species, which is quickly transformed into the DOM and formate species. Afterwards, O_2 is adsorbed and dissociated into O atoms on the Rh cluster surface, which accelerates the formation of formates by interacting with the adsorbed HCHO molecule or DOM. These O atoms would also react with H_2O adsorbed on the proximity of the Rh subnano clusters to produce OH species. Finally, the formate species are oxidized by the OH groups to produce CO_2 and H_2O. The existence and maintenance of OH groups in the presence of O_2 and H_2O are necessary for HCHO oxidation with lower activation energy, which result in good stability of this Rh/TiO_2 catalyst for the oxidation of HCHO.

5. Conclusion

In summary, a catalyst of subnanometer Rh species dispersed on TiO_2 with loading of 1.5 wt% was found for the first time to exhibit excellent performance with complete conversion and good stability in the HCHO oxiation at room temperature. Such high performance can be attributed to the Rh subnano clusters, the support TiO_2 and the formation of surface hydroxyls during the reaction. Various characterizations demonstrated that formates and DOM species were the dominant intermediates after the adsorption of HCHO molecules on the TiO_2 surface, the step of which was accelerated by the adsorbed O atoms on the Rh sites. These intermediates were oxidized into the final products by the OH species which came from the reaction of atomic O and adsorbed H_2O. Moreover, the OH species faciliated the decomposition of formates with lower activation energy and better stability than the O species. This work demonstrated an obvious size-dependent effect of Rh species for ambient oxidation of HCHO from the viewpoint of basic research. Furthermore, the study of subnanometer Rh/TiO_2 catalyst with the ability of effective HCHO removal as well as the good durability and tolerance of moisture can provide important implications for the practical applications and arouse interest in the design of more

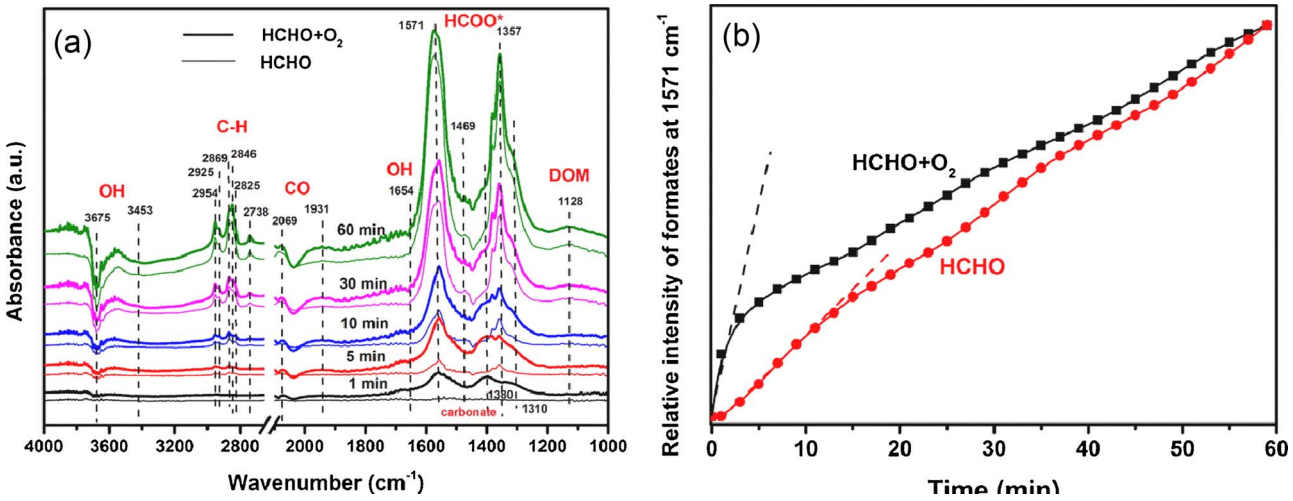

Fig. 12. (a) In situ DRIFT spectra by introducing HCHO + O_2 and HCHO with time on stream on 1.5 wt% Rh/TiO_2 at room temperature, respectively; (b) Dynamic evolution of the integrated area of typical formates peak at 1571 cm^{-1} from (a).

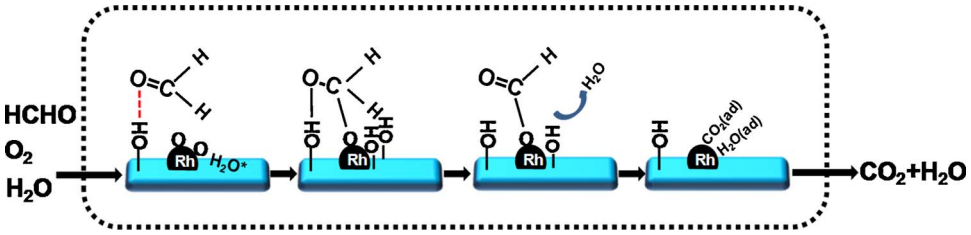

Fig. 13. Schematic of proposed reaction pathway for complete oxidation of HCHO in the presence of H_2O over Rh/TiO_2 at room temperature.

economic Rh-based catalysts with lower loadings for indoor HCHO elimination, such as preparing more uniform subnanometer Rh species or the support rich of hydroxyl species.

Acknowledgments

This work was supported by National Key R&D Program of China (2016YFA0202801), the Strategic Priority Research Program of the Chinese Academy of Sciences (XDB17020100), National Natural Science Foundation of China (21203181, 21576251, 21573232, 21676269), the Youth Innovation Promotion Association CAS (2017223).

References

[1] T. Salthammer, S. Mentese, R. Marutzky, Formaldehyde in the indoor environment, Chem. Rev. 110 (2010) 2536–2572.
[2] IARC, IARC Classifies Formaldehyde as Carcinogenic to Humans, International Agency for Research on Cancer Lyon, 2004 Press Release no. 153.
[3] M. Hakim, Y.Y. Broza, O. Barash, N. Peled, M. Phillips, A. Amann, H. Haick, Volatile organic compounds of lung cancer and possible biochemical pathways, Chem. Rev. 112 (2012) 5949–5966.
[4] S. Brosillon, M.-H. Manero, J.-N. Foussard, Mass transfer in VOC adsorption on zeolite: experimental and theoretical breakthrough curves, Environ. Sci. Technol. 35 (2001) 3571–3575.
[5] K.J. Lee, N. Shiratori, G.H. Lee, J. Miyawaki, I. Mochida, S.-H. Yoon, J. Jang, Activated carbon nanofiber produced from electrospun polyacrylonitrile nanofiber as a highly efficient formaldehyde adsorbent, Carbon 48 (2010) 4248–4255.
[6] Y. Lu, D. Wang, C. Ma, H. Yang, The effect of activated carbon adsorption on the photocatalytic removal of formaldehyde, Build. Environ. 45 (2010) 615–621.
[7] N. Yao, K. Lun Yeung, Investigation of the performance of TiO_2 photocatalytic coatings, Chem. Eng. J. 167 (2011) 13–21.
[8] P. Fu, P. Zhang, J. Li, Photocatalytic degradation of low concentration formaldehyde and simultaneous elimination of ozone by-product using palladium modified TiO_2 films under $UV_{254+185}$ nm irradiation, Appl. Catal. B 105 (2011) 220–228.
[9] J. Mo, Y. Zhang, Q. Xu, J.J. Lamson, R. Zhao, Photocatalytic purification of volatile organic compounds in indoor air: a literature review, Atmos. Environ. 43 (2009) 2229–2246.
[10] X. Tang, J. Chen, X. Huang, Y. Xu, W. Shen, Pt/MnOx–CeO_2 catalysts for the complete oxidation of formaldehyde at ambient temperature, Appl. Catal. B 81 (2008) 115–121.
[11] J. Quiroz Torres, S. Royer, J.P. Bellat, J.M. Giraudon, J.F. Lamonier, Formaldehyde: catalytic oxidation as a promising soft way of elimination, ChemSusChem 6 (2013) 578–592.
[12] L. Nie, J. Yu, M. Jaroniec, F.F. Tao, Room-temperature catalytic oxidation of formaldehyde on catalysts, Catal. Sci. Technol. 6 (2016) 3649–3669.
[13] B. Bai, Q. Qiao, J. Li, J. Hao, Progress in research on catalysts for catalytic oxidation of formaldehyde, Chin. J. Catal. 37 (2016) 102–122.
[14] X. Tang, Y. Li, X. Huang, Y. Xu, H. Zhu, J. Wang, W. Shen, MnO_x–CeO_2 mixed oxide catalysts for complete oxidation of formaldehyde: Effect of preparation method and calcination temperature, Appl. Catal. B 62 (2006) 265–273.
[15] L. Zhu, J. Wang, S. Rong, H. Wang, P. Zhang, Cerium modified birnessite-type MnO_2 for gaseous formaldehyde oxidation at low temperature, Appl. Catal. B 211 (2017) 212–221.
[16] B. Bai, H. Arandiyan, J. Li, Comparison of the performance for oxidation of formaldehyde on nano-Co_3O_4, 2D-Co_3O_4, and 3D-Co_3O_4 catalysts, Appl. Catal. B 142–143 (2013) 677–683.
[17] J. Quiroz, J.-M. Giraudon, A. Gervasini, C. Dujardin, C. Lancelot, M. Trentesaux, J.-F. Lamonier, Total oxidation of formaldehyde over MnOx-CeO_2 catalysts: the effect of acid treatment, ACS Catal. 5 (2015) 2260–2269.
[18] C. Ma, D. Wang, W. Xue, B. Dou, H. Wang, Z. Hao, Investigation of formaldehyde oxidation over Co_3O_4-CeO_2 and Au/Co_3O_4-CeO_2 catalysts at room temperature: effective removal and determination of reaction mechanism, Environ. Sci. Technol. 45 (2011) 3628–3634.
[19] Y. Shen, X. Yang, Y. Wang, Y. Zhang, H. Zhu, L. Gao, M. Jia, The states of gold species in CeO_2 supported gold catalyst for formaldehyde oxidation, Appl. Catal. B 79 (2008) 142–148.
[20] H. Huang, D.Y.C. Leung, Complete elimination of indoor formaldehyde over supported Pt catalysts with extremely low Pt content at ambient temperature, J. Catal. 280 (2011) 60–67.
[21] N. An, Q. Yu, G. Liu, S. Li, M. Jia, W. Zhang, Complete oxidation of formaldehyde at ambient temperature over supported Pt/Fe_2O_3 catalysts prepared by colloid-deposition method, J. Hazard. Mater. 186 (2011) 1392–1397.
[22] S.J. Park, I. Bae, I.-S. Nam, B.K. Cho, S.M. Jung, J.-H. Lee, Oxidation of formaldehyde over Pd/Beta catalyst, Chem. Eng. J. 195–196 (2012) 392–402.
[23] Y. Li, C. Zhang, J. Ma, M. Chen, H. Deng, H. He, High temperature reduction dramatically promotes Pd/TiO_2 catalyst for ambient formaldehyde oxidation, Appl. Catal. B 217 (2017) 560–569.
[24] Z. Huang, X. Gu, Q. Cao, P. Hu, J. Hao, J. Li, X. Tang, Catalytically active single-atom sites fabricated from silver particles, Angew. Chem. Int. Ed. 51 (2012) 4198–4203.
[25] C. Zhang, H. He, K.-i. Tanaka, Perfect catalytic oxidation of formaldehyde over a Pt/TiO_2 catalyst at room temperature, Catal. Commun. 6 (2005) 211–214.
[26] C. Zhang, F. Liu, Y. Zhai, H. Ariga, N. Yi, Y. Liu, K. Asakura, M. Flytzani-Stephanopoulos, H. He, Alkali-metal-promoted Pt/TiO_2 opens a more efficient pathway to formaldehyde oxidation at ambient temperatures, Angew. Chem. Int. Ed. 51 (2012) 9628–9632.
[27] Z. Yan, Z. Xu, J. Yu, M. Jaroniec, Enhanced formaldehyde oxidation on CeO_2/AlOOH-supported Pt catalyst at room temperature, Appl. Catal. B 199 (2016) 458–465.
[28] Z. Xu, J. Yu, M. Jaroniec, Efficient catalytic removal of formaldehyde at room temperature using AlOOH nanoflakes with deposited Pt, Appl. Catal. B 163 (2015) 306–312.
[29] Z. Yan, Z. Xu, J. Yu, M. Jaroniec, Highly active mesoporous ferrihydrite supported Pt catalyst for formaldehyde removal at room temperature, Environ. Sci. Technol. 49 (2015) 6637–6644.
[30] T. Yang, Y. Huo, Y. Liu, Z. Rui, H. Ji, Efficient formaldehyde oxidation over nickel hydroxide promoted Pt/γ-Al_2O_3 with a low Pt content, Appl. Catal. B 200 (2017) 543–551.
[31] B. Chen, X. Zhu, M. Crocker, Y. Wang, C. Shi, FeOx-supported gold catalysts for catalytic removal of formaldehyde at room temperature, Appl. Catal. B 154–155 (2014) 73–81.
[32] C. Zhang, Y. Li, Y. Wang, H. He, Sodium-promoted Pd/TiO_2 for catalytic oxidation of formaldehyde at ambient temperature, Environ. Sci. Technol. 48 (2014) 5816–5822.
[33] J. Peng, S. Wang, Performance and characterization of supported metal catalysts for complete oxidation of formaldehyde at low temperatures, Appl. Catal. B 73 (2007) 282–291.
[34] C. Zhang, H. He, A comparative study of TiO_2 supported noble metal catalysts for the oxidation of formaldehyde at room temperature, Catal. Today 126 (2007) 345–350.
[35] M. Haruta, Size- and support-dependency in the catalysis of gold, Catal. Today 36 (1997) 153–166.
[36] B. Qiao, A. Wang, X. Yang, L.F. Allard, Z. Jiang, Y. Cui, J. Liu, J. Li, T. Zhang, Single-atom catalysis of CO oxidation using Pt_1/FeOx, Nat. Chem. 3 (2011) 634–641.
[37] J. Lin, A. Wang, B. Qiao, X. Liu, X. Yang, X. Wang, J. Liang, J. Li, J. Liu, T. Zhang, Remarkable performance of Ir_1/FeOx single-atom catalyst in water gas shift reaction, J. Am. Chem. Soc. 135 (2013) 15314–15317.
[38] J. Lin, B. Qiao, L. Li, H. Guan, C. Ruan, A. Wang, W. Zhang, X. Wang, T. Zhang, Remarkable effects of hydroxyl species on low-temperature CO (preferential) oxidation over Ir/Fe$(OH)_x$ catalyst, J. Catal. 319 (2014) 142–149.
[39] B. Qiao, J. Lin, L. Li, A. Wang, J. Liu, T. Zhang, Highly active small palladium clusters supported on ferric hydroxide for carbon monoxide-tolerant hydrogen oxidation, ChemCatChem 6 (2014) 547–554.
[40] H. Guan, J. Lin, B. Qiao, X. Yang, L. Li, S. Miao, J. Liu, A. Wang, X. Wang, T. Zhang, Catalytically active Rh sub-Nanoclusters on TiO_2 for CO oxidation at cryogenic temperatures, Angew. Chem. Int. Ed. 55 (2016) 2820–2824.
[41] M. Lin, X. Yu, X. Yang, K. Li, M. Ge, J. Li, Highly active and stable interface derived from Pt supported on Ni/Fe layered double oxides for HCHO oxidation, Catal. Sci. Technol. 7 (2017) 1573–1580.
[42] C. Zhang, H. He, K.-i. Tanaka, Catalytic performance and mechanism of a Pt/TiO_2 catalyst for the oxidation of formaldehyde at room temperature, Appl. Catal. B 65 (2006) 37–43.
[43] S.S. Kim, K.H. Park, S.C. Hong, A study on HCHO oxidation characteristics at room temperature using a Pt/TiO_2 catalyst, Appl. Catal. A 398 (2011) 96–103.
[44] L. Li, J. Lin, X. Li, A. Wang, X. Wang, T. Zhang, Adsorption/reaction energetics measured by microcalorimetry and correlated with reactivity on supported catalysts: a review, Chin. J. Catal. 37 (2016) 2039–2052.
[45] Seiichiro Imamura, Yasuo Uematsu, K. Utani, Combustion of formaldehyde on ruthenium/cerium(IV) oxide catalyst, Ind. Eng. Chem. Res. 30 (1991) 18–21.

[46] Brian E. Spiewak, J.A. Dumesic, Applications of adsorption microcalorimetry for the characterization of metal-based catalysts, Thermochim. Acta 312 (1998) 95–104.
[47] Handbook of Chemistry and Physics, 84th ed., Boca Raton, FL, 2003–2004.
[48] G.Y. Popova, T.V. Andrushkevich, Y.A. Chesalov, E.S. Stoyanov, In situ FTIR study of the adsorption of formaldehyde, formic acid, and methyl formiate at the surface of TiO_2 (Anatase), Kinet. Catal. 41 (2000) 805–811.
[49] J. Rasko, Adsorption and reaction of formaldehyde on TiO_2-supported Rh catalysts studied by FTIR and mass spectrometry, J. Catal. 226 (2004) 183–191.
[50] X. Zhu, J. Yu, C. Jiang, B. Cheng, Catalytic decomposition and mechanism of formaldehyde over Pt-Al_2O_3 molecular sieves at room temperature, Phys. Chem. Chem. Phys 19 (2017) 6957–6963.
[51] Z. Yan, Z. Xu, B. Cheng, C. Jiang, Co_3O_4 nanorod-supported Pt with enhanced performance for catalytic HCHO oxidation at room temperature, Appl. Surf. Sci. 404 (2017) 426–434.
[52] H.F. Wang, R. Kavanagh, Y.L. Guo, Y. Guo, G.Z. Lu, P. Hu, Structural origin: water deactivates metal oxides to CO oxidation and promotes low-temperature CO oxidation with metals, Angew. Chem. Int. Ed. 51 (2012) 6657–6661.
[53] X. Zhu, B. Cheng, J. Yu, W. Ho, Halogen poisoning effect of Pt-TiO_2 for formaldehyde catalytic oxidation performance at room temperature, Appl. Surf. Sci. 364 (2016) 808–814.
[54] H. Huang, P. Hu, H. Huang, J. Chen, X. Ye, D.Y.C. Leung, Highly dispersed and active supported Pt nanoparticles for gaseous formaldehyde oxidation: influence of particle size, Chem. Eng. J. 252 (2014) 320–326.
[55] L. Zhang, L. Chen, Y. Li, Y. Peng, F. Chen, L. Wang, C. Zhang, X. Meng, H. He, F.-S. Xiao, Complete oxidation of formaldehyde at room temperature over an Al-rich Beta zeolite supported platinum catalyst, Appl. Catal. B 219 (2017) 200–208.
[56] L. Wang, H. Yue, Z. Hua, H. Wang, X. Li, L. Li, Highly active Pt/Na_x TiO_2 catalyst for low temperature formaldehyde decomposition, Appl. Catal. B 219 (2017) 301–313.
[57] C. Li, K. Domen, K.i. Maruya, T. Onishi, Spectroscopic identification of adsorbed species derived from adsorption and decomposition of formic acid, methanol, and formaldehyde on cerium oxide, J. Catal. 125 (1990) 445–455.
[58] M.J. van der Niet, A. den Dunnen, L.B. Juurlink, M.T. Koper, Co-adsorption of O and H_2O on nanostructured platinum surfaces: does OH form at steps? Angew. Chem. Int. Ed. 49 (2010) 6572–6575.
[59] L. Xu, Z. Wu, Y. Zhang, B. Chen, Z. Jiang, Y. Ma, W. Huang, Hydroxyls-involved interfacial CO oxidation catalyzed by FeO_x (111) monolayer islands supported on Pt (111) and the unique role of oxygen vacancy, J. Phys. Chem. C 115 (2011) 14290–14299.